Predicting the electrokinetic properties of the crude oil/brine interface for enhanced oil recovery in low salinity water flooding

Miku Takeya [1], Mai Shimokawara [1, 2], Elakneswaran Yogarajah [1, *], Toyoharu Nawa [3], Satoru Takahashi [2]

[1] Division of Sustainable Resources Engineering
Faculty of Engineering, Hokkaido University
Kita 13, Nishi 8, Kita-ku, Sapporo, 060-8628, Japan

[2] Japan Oil, Gas and Metals National Corporation (JOGMEC)
Technology Department
Oil & Gas Upstream Technology Unit
1-2-2 Hamada, Mihama-ku Chiba-city, Chiba, 261-0025, Japan

[3] Hokkaido University
Kita 8, Nishi 5, Kita-ku, Sapporo, 060-0808, Japan

* Corresponding author
E-mail: elakneswaran@eng.hokudai.ac.jp
Tel: +81-11-706-7274

Highlights

- ✧ A triple-layer surface complexation model is proposed for the crude oil/brine interface.
- ✧ The electrokinetic properties are determined and verified by experimental data.
- ✧ The ions' affinity toward the crude oil follows the order: Ca^{2+} <Mg^{2+} <OH^-.
- ✧ Electrical triple-layer expansion impacts more than just the surface charge at the crude oil/brine interface for EOR in LSWF.

Graphical abstract

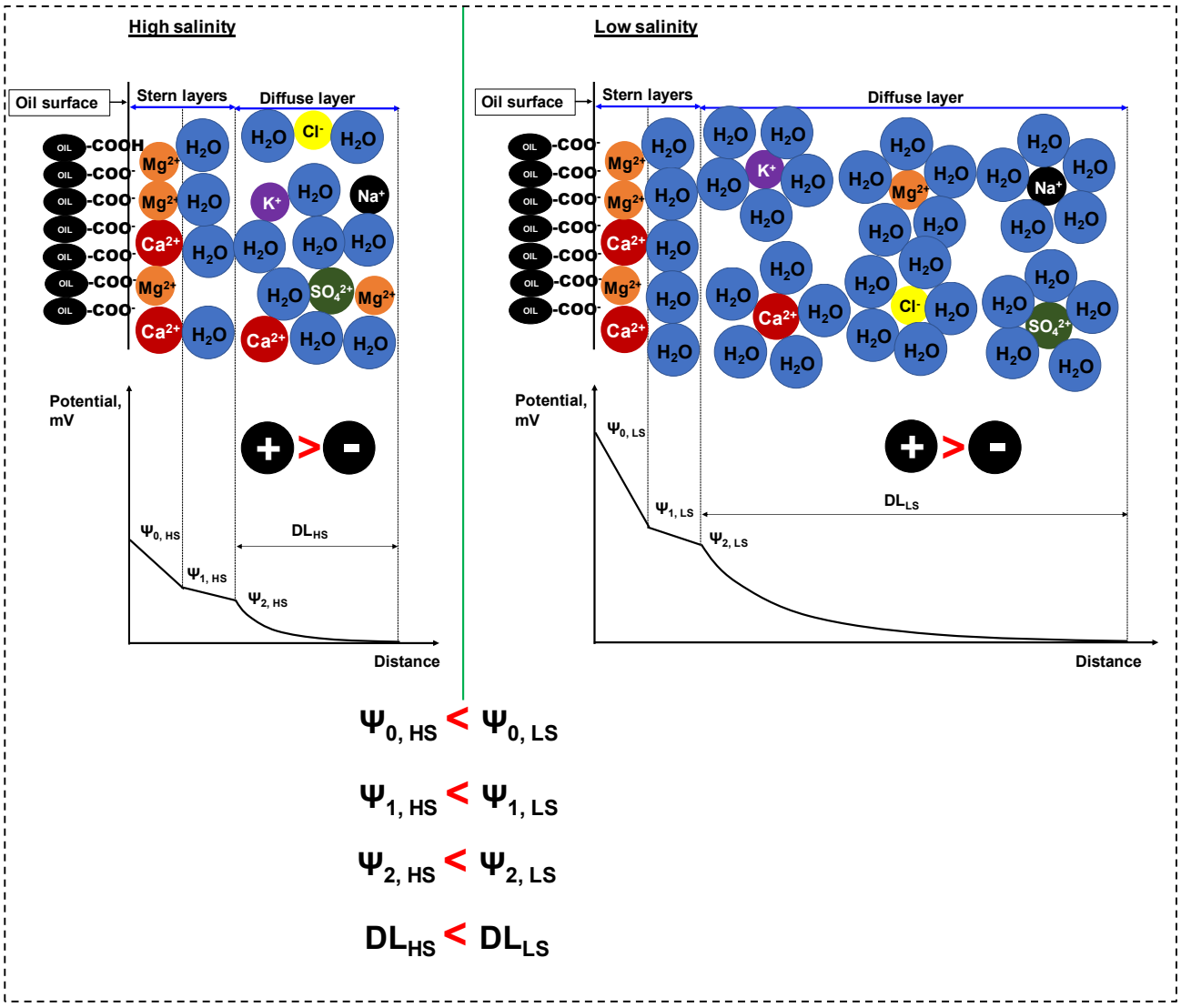

Abstract

The low-salinity waterflooding (LSWF) technique during enhanced oil recovery has received increasing attention over the last decade. Several studies have attempted to understand the effects of LSWF through both experiments and modelling, but their results are inconsistent due to a lack of understanding of the crude oil/brine and brine/rock interfaces. In this paper, the crude oil/brine interface was studied by developing a triple-layer surface complexation model. The carboxyl groups (-COOH) were attributed to the surface charge and electrical triple-layer development of the crude oil in LSWF. The zeta potentials of the emulsion at various pH levels and the calcium and magnesium concentrations were measured to examine the interface. These data were then directly fitted to the simulated zeta potentials to determine the surface site density of -COOH and the associated equilibrium constants for the dissociation and adsorption of calcium and magnesium. The -COOH site density was determined by fitting the pH-independent zeta potential, while the equilibrium constant values were estimated from the variations in the zeta potential with the changes in pH and the concentrations of calcium and magnesium. The determined surface complexation parameters were validated by comparing the experimental zeta potential data from different ionic solutions. The developed surface complexation model was used along with the estimated parameters to predict the interface of crude oil in seawater, formation water, and their dilutions. The simulated zeta potential results agreed well with the experimental data, demonstrating that the model is applicable to understand the crude oil/brine interface in LSWF. Finally, the importance of the prediction of the surface and zeta potentials in the evaluation of the interface and the estimation of electrostatic forces, and thus the wettability alteration, was discussed.

Keywords: Zeta potential; Electrical triple-layer; Surface complexation model; Low salinity water; IOR/EOR

1. Introduction

Over 65% of oil persists after the first and second recovery processes; therefore, a cost-effective and environment-friendly method of oil recovery is necessary to meet the increasing energy demand. Many researchers and industries have been investigating a variety of Enhanced Oil Recovery (EOR) techniques to meet the demand for oil [1–4]. Low salinity water flooding (LSWF), or smart water flooding, has recently received interest as an economical EOR method, which involves the injection of low-salinity brine, such as seawater or formation water, into a reservoir under secondary or tertiary conditions [1–12]. Several field and laboratory experiments and simulations have demonstrated improved oil recovery by LSWF after the secondary recovery [5–12], but some have not [13]. Oil recovery by LSWF is strongly dependent on the types of brines used and their salinity [7–11, 14]. Therefore, a clear understanding of the crude oil/brine and rock/brine interfaces is essential for determining the effect of LSWF on EOR.

Various mechanisms have been suggested that could explain the effect of LSWF such as, fines migration and permeability reduction, pH, mineral dissolution, osmotic effects, desorption of polar oil components, micro-dispersion formation, viscoelasticity, expansion of the electrical double layer (EDL), multi component ionic exchange (MIE), and wettability alteration [1–4, 15–20]. Although several mechanisms have been proposed, the dominant mechanisms are still unclear. Researchers have recently agreed that wettability alteration is the most accepted mechanism regarding the effect of LSWF [1, 18–21], and that EDL expansion, MIE, and electrostatic repulsion between the crude oil/brine and brine/rock interfaces can alter the wettability. The polar components of crude oil are adsorbed to the rock's surface, through divalent cation bridging or directly to the surface. A decrease in the salinity expands the EDL between the crude oil and rock surfaces, and also removes cations adsorbed on the rock's surface, resulting in the release of adsorbed oil. In addition, lowering the salinity creates more negative oil/brine and rock/brine surfaces, which increases the repulsive forces

between them. These LSWF effects alter the wettability from oil-wet to mixed-wet or mixed-wet to water-wet, increasing the release of oil from rock surfaces [18–21].

Wettability alteration strongly depends on the surface electrical charge at the crude oil/brine and rock/brine interfaces: oppositely charged surfaces attract one another, while the same surface charges generate a highly repulsive force. The surface charges of the interfaces are closely related to the measurable zeta potential, which is the electrical potential at the slipping plane of the EDL. The ionic strength and types of ions in the solution affect the zeta potential, and subsequently affecting the thickness of the EDL and the surface charge, which alter the wettability of the crude oil-brine-rock system. Several studies have investigated the impacts of pH, ionic strength, and cation type on the zeta potential of the crude oil and rock surface and have related the potential to the adsorption and desorption of crude oil on the rock surface [21–27]. However, the measurable zeta potential differs from the surface potential, which cannot be measured. The surface potential has been formulated in various theories, such as Derjaguin–Landau–Verwey–Overbeek (DLVO) theory, to understand the interface and its interactions, but many studies have used the measured zeta potential instead of the surface potential to calculate the electrostatic forces in the DLVO theory and explain the changes in the disjoining pressure due to varying brine composition [27–29]. Therefore, separate computation of the surface and zeta potentials is necessary to understand the electrostatic interactions between the crude oil/brine and brine/rock interfaces.

Surface complexation models provide insight into the surface coordination reactions at the crude oil/brine and brine/rock interfaces. Diffuse double-layer surface complexation models have been used to predict the impact of the brine composition on the adsorption and desorption of crude oil and double layer expansion [12, 30–35]. Although the diffuse double layer model allows the prediction of the surface behaviour of the interfaces, it cannot directly compare the measured zeta potential of the interfaces at different solution compositions as it can only predict the surface potential. Therefore,

the main objective of this study is to propose an electrical triple-layer surface complexation model for the crude oil/brine interface. The surface chemistry of both the crude oil/brine and rock/brine interfaces affects the oil recovery in LSWF, but this study only focuses on the crude oil/brine interface. A methodology is proposed to determine the surface complexation modelling parameters, such as the density of surface functional groups of the crude oil and the equilibrium constants for the surface species interaction with pH, calcium, and magnesium. The surface complexation modelling results were compared with the measured zeta potential for the crude oil emulsion in different solutions to validate the model and the determined surface complexation modelling parameters. Finally, the proposed model is used to explain the behaviour of the crude oil/brine interface in terms of wettability alteration in LSWF.

2. Materials and methods

2.1 Experimental

The properties of the crude oil used in the experiment are given in **Table 1**. It should be noted that this crude oil has waxy characteristics, which can fluidify above 35 ºC and solidify at room temperature. Very recent research has investigated the effect of LSWF in waxy crude oil [36]. Sample preparation and the experiments were conducted at 50 ºC. The electrolyte solutions used in the experiments were prepared by mixing the chemical reagents with deionised water. In this study, NaOH, NaCl, $CaCl_2$, and $MgCl_2$ solutions with different concentrations were used. Further, formation water and seawater were prepared using NaCl, $CaCl_2{:}2H_2O$, $MgCl_2{:}6H_20$, Na_2SO_4, and $NaHCO_3$, and then diluted 3, 7, 20, and 30 times using deionised water. The concentrations of the prepared formation water and seawater are presented in **Table 2**.

The zeta potential of the crude oil/brine interface was measured using Zeta-potential & Particle size analyser ELSZ-1000, manufactured by Otsuka Electronics. All zeta potential measurements were conducted at 50 ºC. The crude oil to solution ratio was constant for each measurement: 0.1 mL (0.5%)

of crude oil in 20 mL of solution. The crude oil and solution were emulsified by mixing the sample with a vortex mixer for one minute and then an ultrasonic cleaner for two minutes. The emulsion was extracted with a syringe and injected into a standard cell for measurement. The pH of each sample was measured before and after the addition of crude oil to the solution using a pH meter.

Table 1

Crude oil properties

Property	**Value**
Density (g/cm^3)	0.818
Viscosity (cP)	8.398
Acid number (mgKOH/g)	0.39
Base number (mgKOH/g)	1.86
Composition	**wt. (%)**
Saturates	46.4
Aromatics	16.9
Resins	12.5
Asphaltenes	24.2

Table 2

Compositions of seawater and formation water used for zeta potential measurement

Ion	Concentration (mg/L)	
	Formation water	Seawater
Na^+	12153	11345
Ca^{2+}	2133	441
Mg^{2+}	320	1075
K^+	137	439
Cl^-	22519	18966

HCO_3^-	141	119
SO_4^{2-}	72	2676

151

152 **2.2 Description of the surface complexation model: CD-MUSIC**

153 The charge distribution-multi site complexation model (CD-MUSIC), built-in geochemical code
154 PHREEQC, is used for the surface complexation calculations [37-39]. This model can be considered
155 as a triple-layer surface complexation model for a single site on one surface. Each ion differs in size
156 and has different interactions towards the charged surface; thus, there are various locations from the
157 surface for the ions. Many studies have highlighted the self-assemblage of oil components at the
158 oil/water interface [40-42]. The accumulation of asphaltenes and resin components or their single
159 molecule forms active surfaces at the interface. The other oil components distribute throughout the
160 oil phase and do not contribute to the formation of active surfaces even if they accumulate at the
161 interface. In this study, the emulsion prepared for zeta potential experiment was assumed to have
162 uniform characteristics, and possible accumulation may not have changed the properties of the active
163 surfaces of the oil components. Therefore, consistent with numerous studies [12, 30–35], the active
164 surfaces of oil components could be treated as a solid surface with a constant site density. The
165 carboxyl groups (-COOH) and nitrogen bases (-N) are the main polar components of the crude oil
166 from asphaltenes and resins and can contribute on the surface charge development of crude oil
167 through the dissociation and adsorption of ions [1, 12, 20, 43]. It was assumed that only the resin
168 components of the oil have -COOH surface groups that controls the surface charge and electrical
169 triple-layer formation at crude oil/brine interface during LSWF, while the nitrogen bases (-N) surface
170 groups were not considered as LSWF in slightly basic or basic conditions, based on previous studies
171 [1, 12].

172

173 On the basis of the results reported on the zeta potential experiments and the diffuse double layer
174 surface complexation model, divalent calcium and magnesium cations and hydroxyl ions are the

potential determining ions in the crude oil/brine interface [12, 25, 27, 30, 31]. The divalent cations lose some of their water molecules and create an innersphere surface complex with the carboxyl groups of crude oil forming a Stern or adsorbed layer, while other ions diffuse through the diffuse layer. The sodium and chloride ions affect surface adsorption by modifying the ionic strength and forming aqueous complexes [12]; thus, they do not directly adsorb on the surface. The triple layer (CD-MUSIC) at the crude oil/solution interface in LSWF is illustrated in **Fig. 1**. The surface has three planes: the 0-, 1-, and 2-planes. The surface groups are located at the 0-plane, and the diffuse layer begins at the 2-plane. The potential at the 0-plane is the surface potential, and the zeta potential can be directly compared to the potential at the 2-plane. The CD-MUSIC model requires the capacitance of the layers and change in charge at three layers due to dissociation of surface sites and adsorption of ions on the sites, in addition to surface site density and equilibrium constants which are needed for double layer model as well. The capacitance of the first (0- to 1-plane) and second (1- to 2-plane) Stern layers can be calculated by [38]

$$C = \frac{\varepsilon_0 \varepsilon_r}{d} \quad (1)$$

where ε_0 and ε_r are the absolute (8.85×10^{-12} $CV^{-1}m^{-1}$) and relative dielectric constants, respectively, and d is the distance between the planes. It is assumed that the dissociation reaction takes place at the 0-plane, whereas the innersphere complex adsorption of calcium and magnesium changes the charge at 0- and 1-planes. Therefore, the distance *d1* is the size of an adsorbed ion: the size of a calcium or magnesium ion for its adsorption or the size of a water molecule for the dissociation of -COOH. The size of a water molecule is considered for the distance *d2*. The positions of the ions in the Stern layers change the charge of three layers. The focus of this study is to determine the surface site density of -COOH and its associated equilibrium constants for the dissociation and adsorption of calcium and magnesium. Thus, the charge distribution at three layers for -COOH dissociation and the adsorption of calcium and magnesium were assumed as given in **Table 3.**

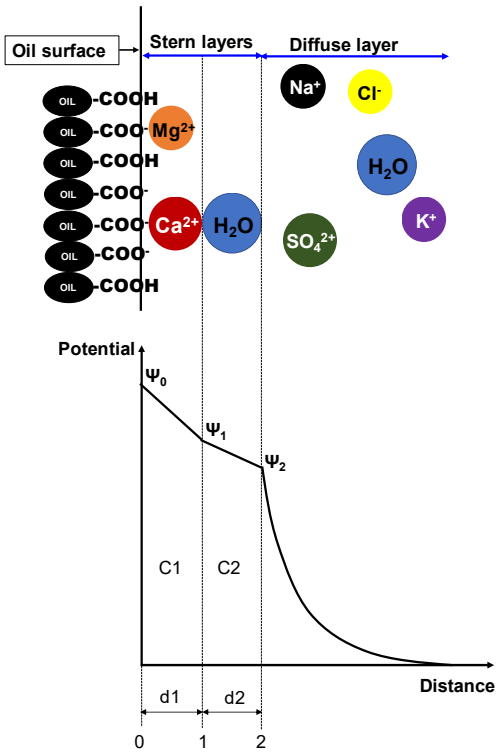

Fig. 1. Schematic of the electrical triple-layer used in the CD-MUSIC model

The dissociation of surface carboxyl groups and the adsorption of divalent cations on the groups can be written as

$$\text{-COOH} \leftrightarrow \text{-COO}^- + \text{H}^+ \qquad K_{COO^-} = \frac{(-COO^-)*(a_{H^+})}{(-COOH)} \exp(-\frac{\Delta z_i F \psi_i}{RT}) \tag{2}$$

$$\text{-COOH} + \text{Ca}^{2+} \leftrightarrow \text{-COOCa}^+ + \text{H}^+ \qquad K_{COOCa^+} = \frac{(-COOCa^+)*(a_{H^+})}{(-COOH)*(a_{Ca^{2+}})} \exp(-\frac{\Delta z_i F \psi_i}{RT}) \tag{3}$$

$$\text{-COOH} + \text{Mg}^{2+} \leftrightarrow \text{-COOMg}^+ + \text{H}^+ \qquad K_{COOMg^+} = \frac{(-COOMg^+)*(a_{H^+})}{(-COOH)*(a_{Mg^{2+}})} \exp(-\frac{\Delta z_i F \psi_i}{RT}) \tag{4}$$

where K_{COO^-}, K_{COOCa^+}, and K_{COOMg^+} are the intrinsic equilibrium constants for dissociation, calcium adsorption and magnesium adsorption, respectively; *(-COO$^-$), (-COOH), (-COOCa$^+$),* and *(-*

215 $COOMg^{+})$ are the concentrations (mol/m^2) of the surface species of the carboxyl groups; a_j is the
216 activity of ionic species j; ψ_i is the potential at the 0-, 1-, or 2-plane (V); Δz_i is the charge distribution;
217 R is the universal gas constant equal to 8.31451 J/(mol.K); and T is the absolute temperature (K). This
218 model is implemented in PHREEQC using the SURFACE and SURFACE_SPECIES keyword data
219 blocks with the specification of charge distribution and the capacitance of the first and second Stern
220 layers [39].
221
222 **Table 3**
223 Charge distribution values for the dissociation and adsorption of calcium and magnesium on
224 carboxylic sites

Ions	Δz_0	Δz_1	Δz_2	**Eq.**
OH^-	-1	0	0	(2)
Ca^{2+}	-1	2	0	(3)
Mg^{2+}	-1	2	0	(4)

225
226 **3. Results and discussion**
227 **3.1 Site density and deprotonation of carboxylic groups: determination and verification**
228 The density of the -COOH surface groups and the equilibrium constant (K_{COO-} in Eq. (2)) value for
229 the dissociation of carboxyl groups were determined from the measured zeta potentials and the results
230 of CD-MUSIC surface complexation modelling. This model can separately predict the surface (at the
231 0-plane) and zeta potentials (at the 2-plane), the latter of which is directly comparable to the measured
232 zeta potential. This is not possible with the diffuse layer surface complexation model that can only
233 predict the surface potential, which is completely different from the zeta potential. The electrical
234 properties of the surface and the solution composition affect the difference between these potentials,
235 which will be discussed in section 3.3.
236

The effects of pH and ionic strength on the zeta potential of crude oil are shown in **Fig. 2**. The pH of the solution was adjusted using NaOH while NaCl was added appropriately to maintain the ionic strength. Therefore, the concentration of Na is constant over the pH and Cl concentration decreases with pH. The increase in the pH enhances the dissociation of -COOH, causing the surface to become more negatively charged. The figure shows that pH does not influence the dissociation above a pH of 9. This is due to the complete dissociation of the -COOH surface groups. The pH required to fully dissociate -COOH depends on the ionic strength: a high ionic strength requires a lower pH to fully dissociate -COOH than that for a low ionic strength. This characteristic is used to determine the density of -COOH. The CD-MUSIC model can predict the zeta potential of the emulsions given the inputs of site density, equilibrium constant (K_{COO^-}), capacitance (C1 and C2), and amount and specific surface area of oil. The specific surface area of oil is calculated from the measured size of the oil particles in the solution, equal to 0.5 m^2/g of resins. C1 and C2 are equal to 2.253 F/m^2, assuming that there is a water molecule (diameter of 2.75Å) attached to the first and second Stern layers (Eq. (1) and **Fig. 1**). Dissociation only changes the charge at the 0-plane (**Table 3**). The measured zeta potential data at an ionic strength of 100 mM were fitted to the predicted values in two different pH ranges. Initially, the simulation was performed with a $log\_K_{COO^-}$ of zero, and the predicted zeta potentials were fitted to the measured values by only changing the -COOH site density in a pH range (above 9) where the zeta potential is independent of pH. The estimated site density was used to fit other zeta potential values (below a pH of 9), where the values are pH-dependent, by only adjusting the $log\_K_{COO^-}$. The determined -COOH site density and $log\_K_{COO^-}$ values are 0.47 sites/nm^2 and -5.6, respectively. The optimised equilibrium constant and site density were obtained when an R^2 value close to one for the plot of experimental versus predicted zeta potential values. This methodology will be used to optimise the equilibrium constants for calcium and magnesium adsorption (section 3.2). The estimated site density and $log\_K_{COO^-}$ values do not differ much from those reported in the literature [12, 30, 31, 33, 34]. These values, together with C1 and C2, were used to predict the zeta potential of the emulsions at the ionic strengths of 20 and 700 mM. The simulation results agree well

263 with the measured zeta potential data at low and high ionic strengths, indicating the predictive
264 capability of the model for LSWF.
265

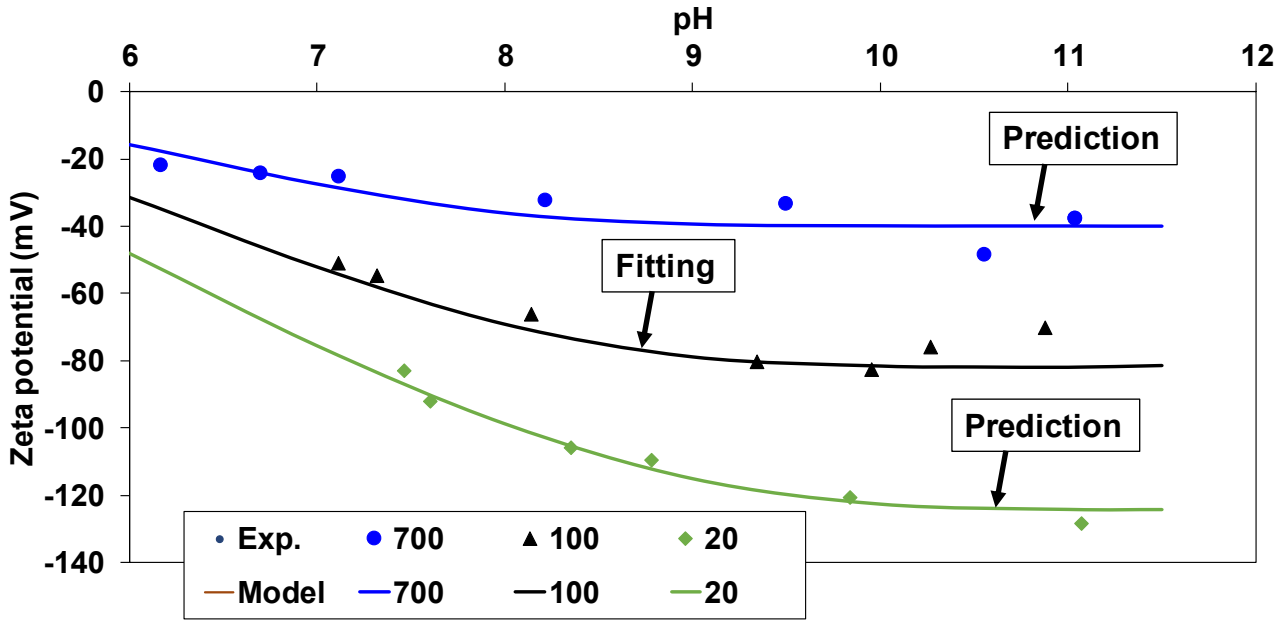

266

267 **Fig. 2.** Measured and predicted zeta potentials of crude oil as a function of pH at ionic strengths of
268 20, 100, and 700 mM. The ionic strength was adjusted with an NaCl solution.
269

270 **3.2 Interactions between calcium and magnesium ions and crude oil: determination of**
271 **equilibrium constants and prediction of zeta potentials**

272 Divalent calcium and magnesium cations can adsorb on the surface of -COOH, and cause both the
273 surface and zeta potentials toward positive. The zeta potentials of crude oil emulsions in solutions
274 with varying $CaCl_2$ concentrations at constant pH values of 8 and 10 and a constant ionic strength of
275 20 mM are shown in **Fig. 3**. The higher pH value was selected considering the dissociation of -COOH,
276 which produces more than 70 % of the $-COO^-$ at a pH of 8 and an ionic strength of 100 mM, and a
277 low ionic strength was selected to understand the adsorption in LSWF. NaOH and NaCl solutions, as
278 in section 3.1, were used to fix the pH and ionic strength, respectively. The addition of calcium to the
279 emulsion dramatically increased the zeta potential, which in turn gradually increased with the calcium
280 concentration. The calcium adsorption on -COOH surfaces was modelled by CD-MUSIC taking the

reactions given in Eqs. (2) and (3) and the charge distribution for calcium adsorption given in **Table 3**. The density of -COOH and the *log_K*$_{COO^-}$ value determined in section 3.1 were used to predict the calcium interactions. The thicknesses of the first and second Stern layers were determined by the respective presence of calcium ions and water molecules in the layers (**Fig. 1**), giving the values of C1 and C2 as 3.098 F/m^2 and 2.253 F/m^2, respectively. The only parameter required to predict the zeta potential of the emulsion in the calcium-containing solution is the *log_K*$_{COOCa^+}$, which was determined by fitting the measured zeta potential values at a pH of 8.0 with the modelling results (**Fig. 3(A)**). A value of -4.7 was obtained for the assumed positions of both calcium ions and water molecules in the Stern layers. To understand the effects of the widths of the first and second Stern layers on *log_K*$_{COOCa^+}$, the fitting was carried out for different cases. The detail of the thicknesses of the Stern layers and the estimated *log_K*$_{COOCa^+}$ values are presented in **Table 4**. The widths of the Stern layers did not significantly affect *log_K*$_{COOCa^+}$; thus, a value of -4.8±0.1 was determined to be the most suitable for *log_K*$_{COOCa^+}$. The interactions between the $CaOH^+$ and -COOH surface groups were not considered as there was very little $CaOH^+$ (less than 1%) in the solution, even at a high $CaCl_2$ concentration and a pH of 10. The calculated surface complexation modeling parameters predicted the measured zeta potentials well at a pH of 10 and an ionic strength of 20 mM (**Figs. 3(B)** and **3(C)**).

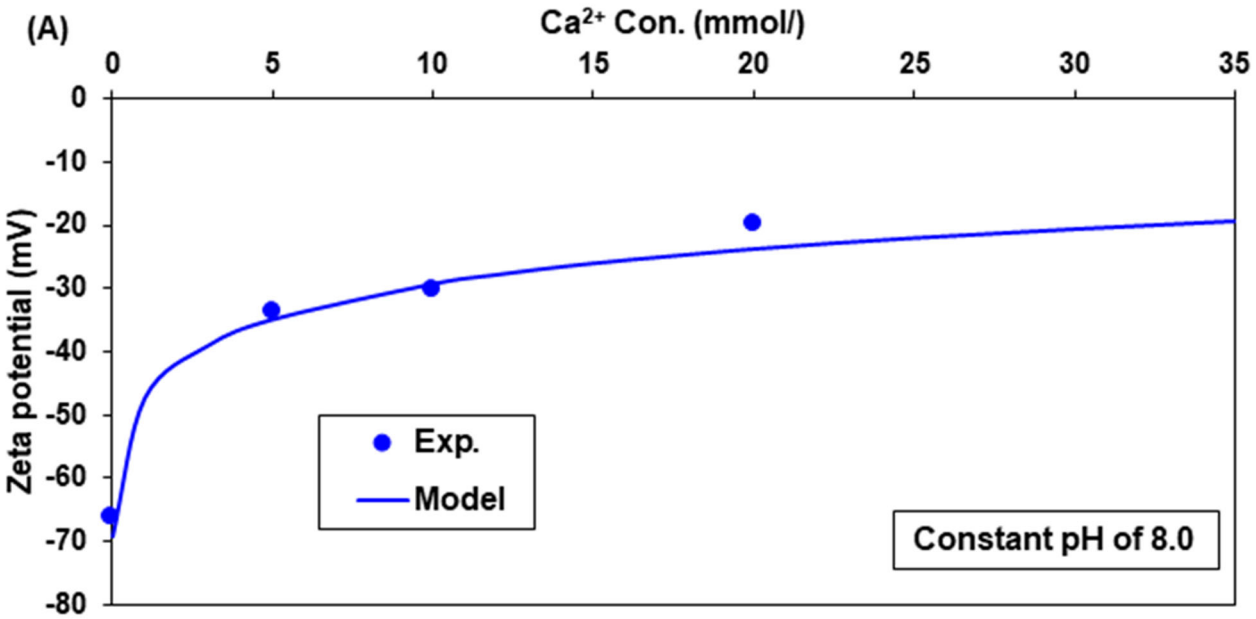

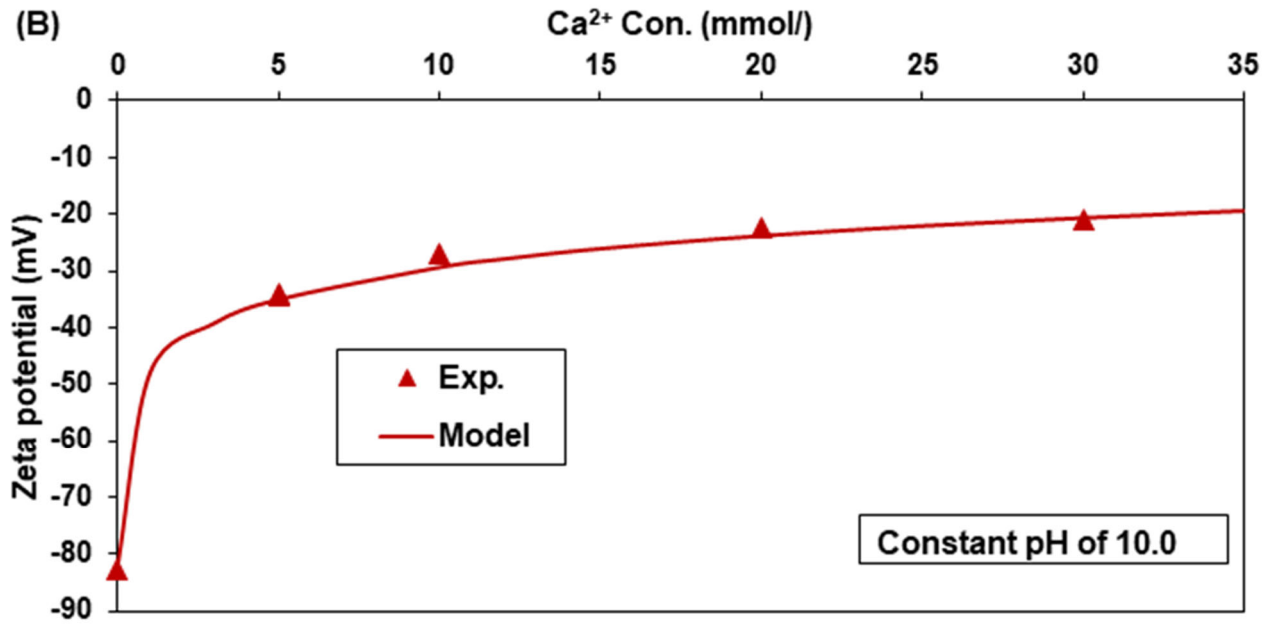

299

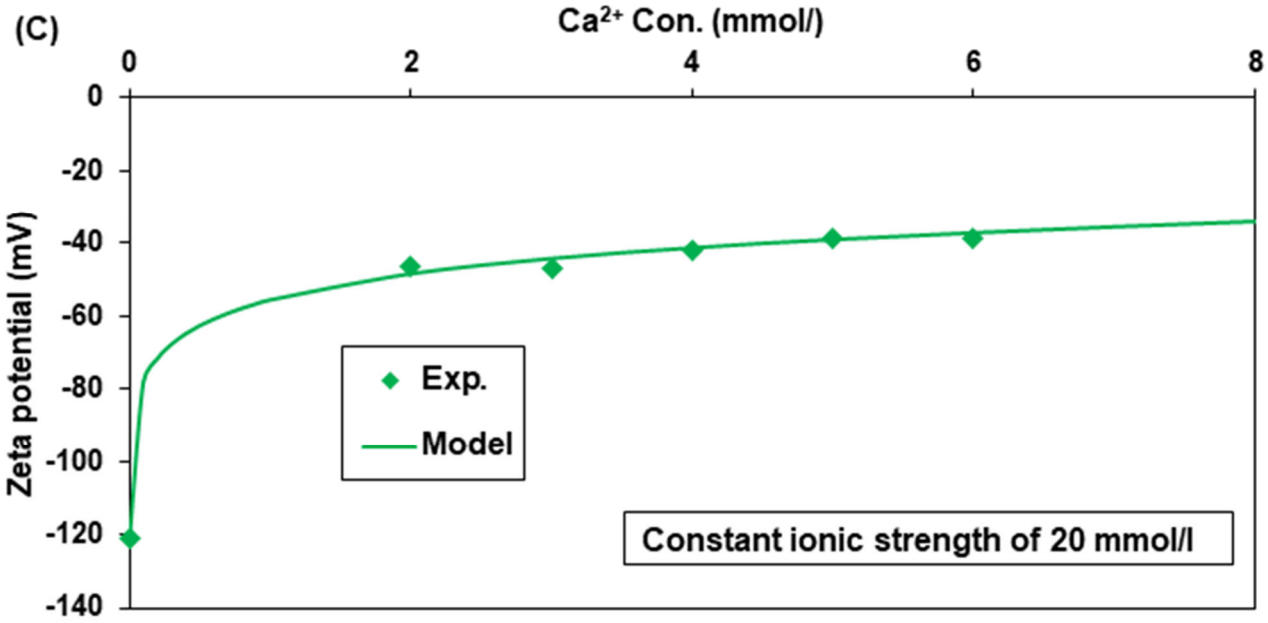

300

301 **Fig. 3.** Measured and predicted zeta potential of crude oil as a function of Ca^{2+} concentration for (A)
302 a constant pH of 8.0; (B) a constant pH of 10.0; and (C) a constant ionic strength of 20 mM. The ionic
303 strength was adjusted with a NaCl solution.

304

305

306

Table 4

Thicknesses of the first and second Stern layers and the estimated log_K_{COOCa+} values for four different scenarios

	d1	**d2**	log_K_{COOCa+}
Case 1	Diameter of calcium	Diameter of water	-4.7
Case 2	Radius of calcium	Radius of calcium + diameter of water	-4.8
Case 3	Diameter of calcium + diameter of water	Diameter of water	-4.7
Case 4	Diameter of calcium + diameter of water	Diameter of water * 2	-4.9

As for calcium, the influence of the magnesium ions on the zeta potential of a crude oil emulsion was also studied. The zeta potential increases with the concentration of magnesium ions for the crude oil in $MgCl_2$ solution at pH levels of 7 and 8 and an ionic strength of 20 mM (**Fig. 4**). A similar tendency was obtained with calcium. To prevent the formation of brucite, a pH below 8 was selected. The simulation was performed in the CD-MUSIC model considering the reaction given in Eq. (4) and the parameters estimated in section 3.1. However, the calculated value of C1 for the adsorption of magnesium on the first Stern layer was 4.302 F/m^2, and C2 was the same as used in the calcium interaction, 2.253 F/m^2. The zeta potential measured at a pH of 8 was used to fit the modelling results and the determined value of log_K_{COOMg+} was -3.85 (**Fig. 4(A)**). As was carried out for calcium (**Table 4**), four different scenarios for the widths of the Stern layers were assumed to estimate the log_K_{COOMg+}, and the most suitable log_K_{COOMg+} was -3.9±0.05. To verify the estimated parameters, the calculation was carried out at a pH of 7 and an ionic strength of 20 mM. As explained for calcium, $MgOH^+$ was not considered in the calculation as it had a negligible concentration in the solution. A comparison between the model-predicted and measured zeta potentials is shown in **Figs. 4(B)** and

4(C). The good agreement between the model-predicted and experimental data for both calcium and magnesium interactions strongly suggests that the estimated surface complexation modeling parameters are applicable for LSWF. Furthermore, both the experimental and modeled zeta potential results show that magnesium ions adsorb onto crude oil with a higher affinity than calcium ions.

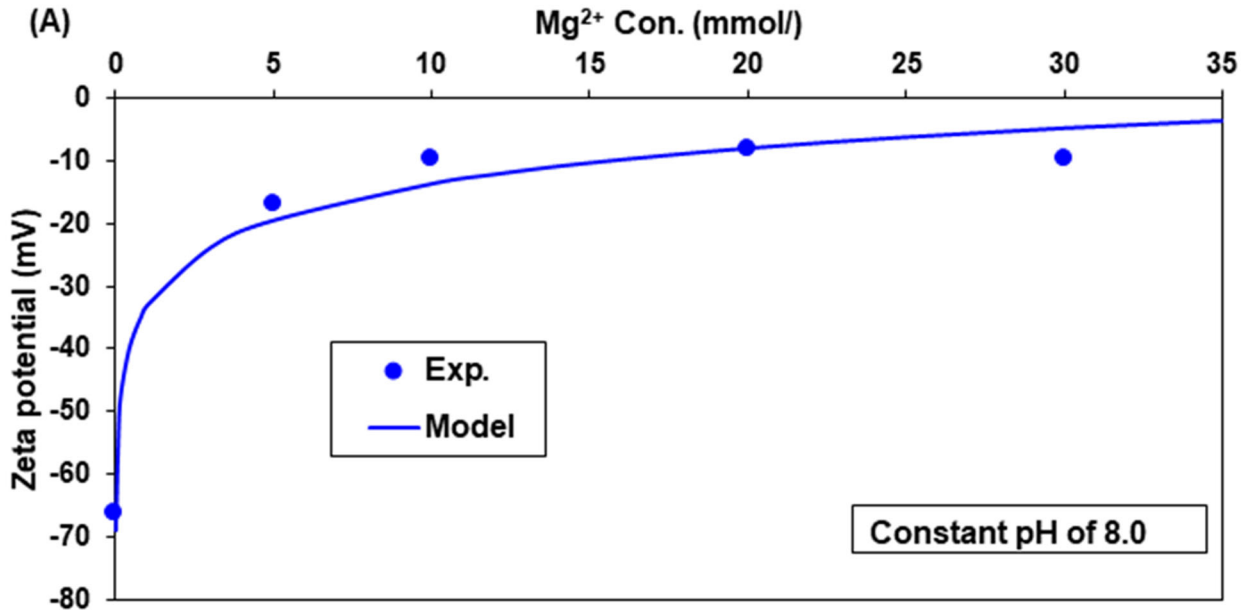

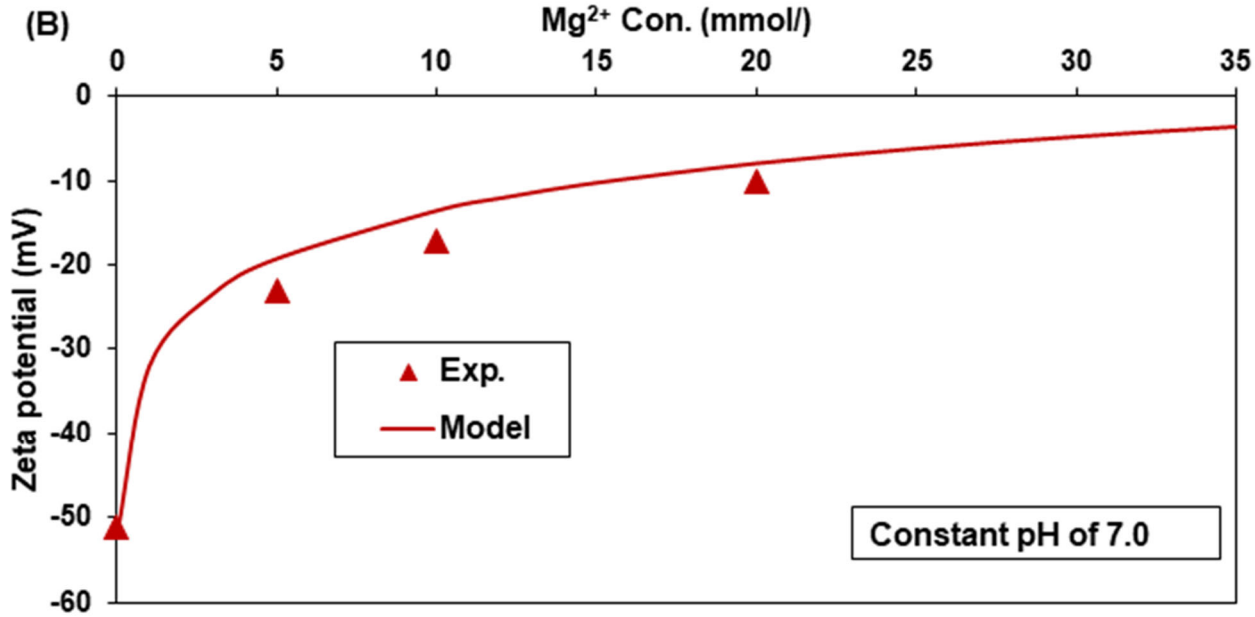

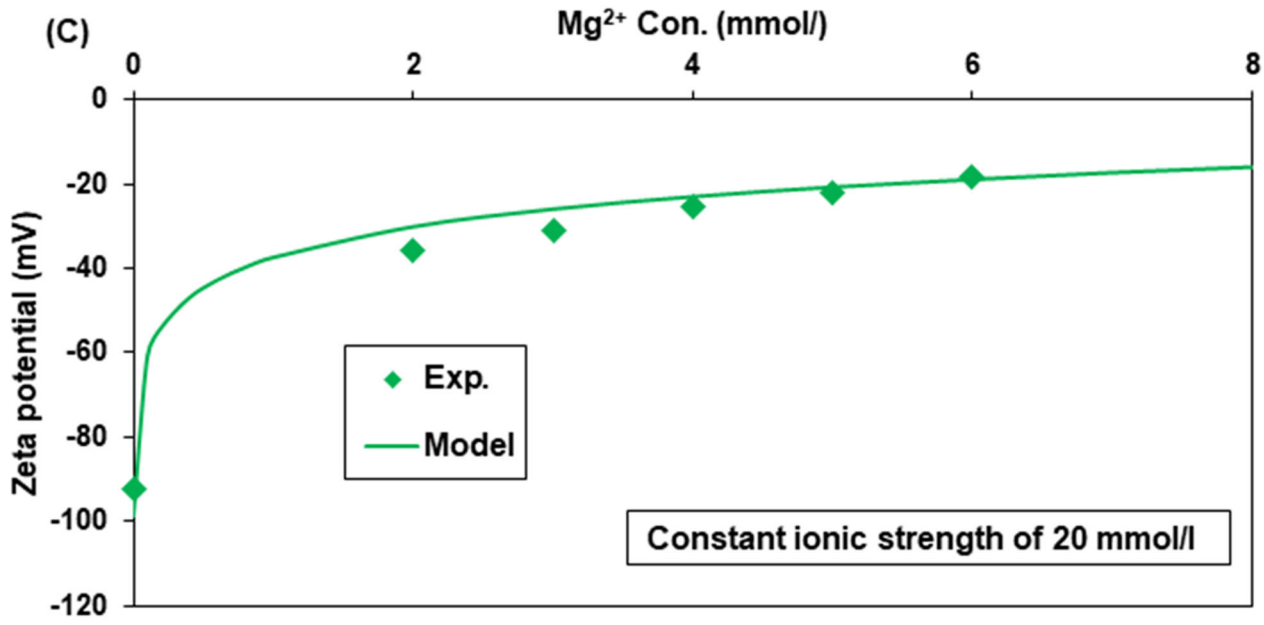

Fig. 4. Measured and predicted zeta potentials of crude oil as a function of Mg^{2+} concentration for (A) a constant pH of 8.0; (B) a constant pH of 7.0; and (C) a constant ionic strength of 20 mM. The ionic strength was adjusted with a NaCl solution.

3.3 Prediction of the zeta potential of crude oil in diluted seawater and formation water

The estimated surface complexation parameters, such as the -COOH surface site density and the equilibrium constants for the dissociation and adsorption of calcium and magnesium ions, in sections 3.1 and 3.2 were used to predict the zeta potentials of the emulsions in seawater, formation water, and their dilutions. Although these solutions consisted of multi-ions (**Table 2**), the pH and divalent cations are the potential-determining ions that strongly impact the electrical triple-layer at the oil/brine interface. The presence of calcium ions, whose hydration radius is higher than that of magnesium ions, and water molecules in the Stern layers determines the values of C1 and C2 (Case 1 in **Table 4**). **Figure 5** compares the experimental zeta potential with the simulation results for emulsions of crude oil with seawater and formation water. The model predictions agreed well with the experimental results. The results indicate that the zeta potential of oil in seawater or formation water is weakly negative owing to the high concentrations of calcium and magnesium. This supports the results described in sections 3.1 and 3.2; the zeta potential does not become positive at a high concentration

because the pH has more of an impact on the zeta potential than the concentration of divalent ions. Furthermore, a reduction in the salinity or dilution causes the zeta potential to become more negative.

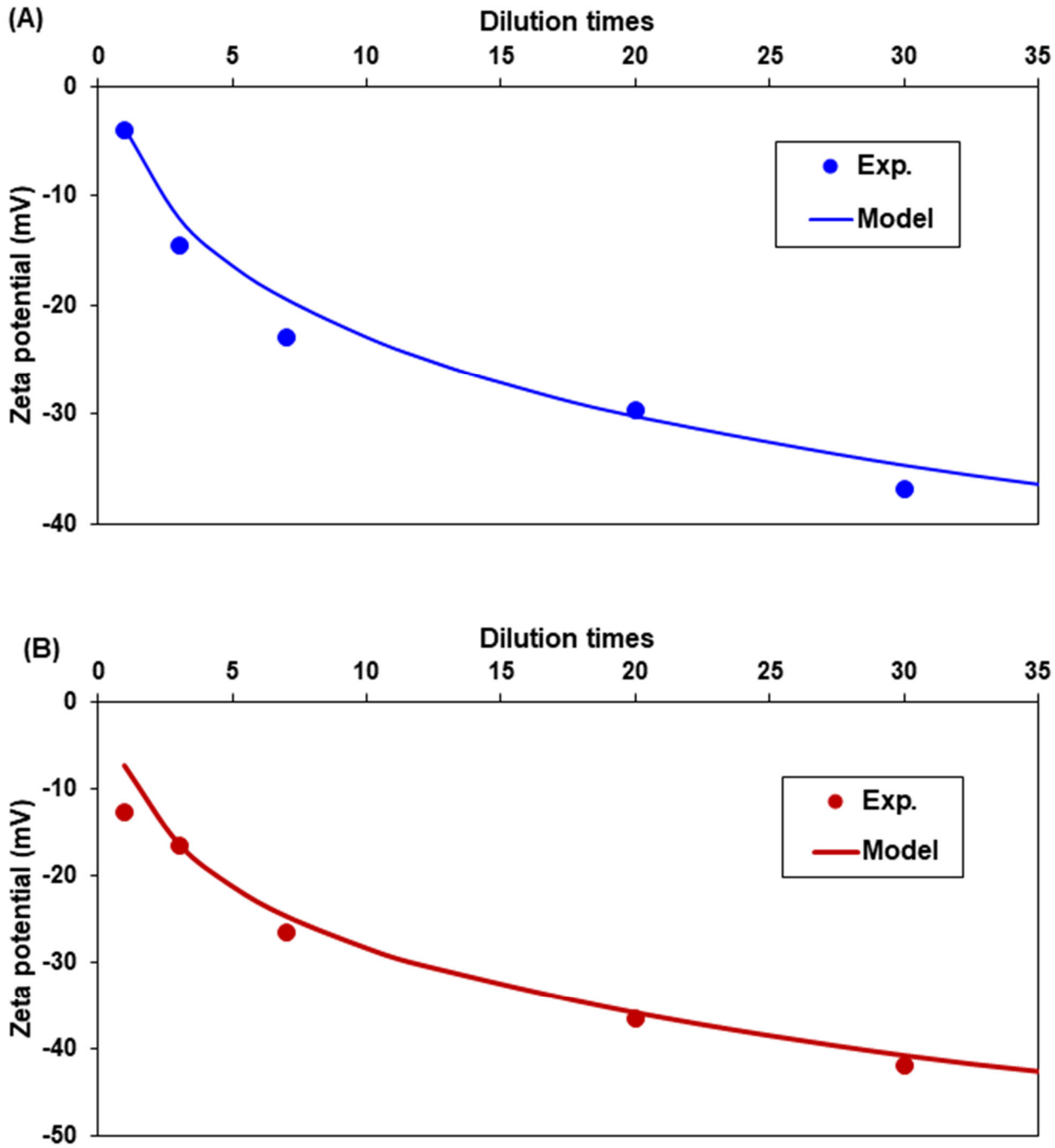

Fig. 5. Comparison of the predicted and measured zeta potentials of crude oil in (A) seawater; (B) formation water, as a function of dilution times.

The surface complexation model was applied to understand the effects of the surface charge and potential at the crude oil/brine interface, which influence the wettability change in LSWF. **Figure 6(A)** compares the computed zeta potential with the surface potential together with the calculated diffuse layer thickness for the crude oil emulsions with seawater and its dilutions. As discussed previously, the measurable zeta potential differs from the surface potential. The absolute surface potential was more than double the zeta potential up to a dilution of 20 times, and the potentials became more negative with increasing dilution. The zeta and surface potentials could be positive and negative, respectively, or vice-versa for different brine compositions, though both potentials were negative in this study. The calculation of the adhesion forces in DLVO theory using the zeta potential values rather than surface potential may cause incorrect prediction. Therefore, the surface potential should be used instead of the zeta potential to evaluate the crude oil/brine interface and hence the wettability alteration.

The concentration or amount of surface species on the -COOH surface affects the surface potential and then the zeta potential. The simulation results of the surface species distribution with reducing seawater salinity are shown in **Fig. 6(B)**. The higher concentration of $-COO^-$ than that of the other species causes negative surface and zeta potentials. The distribution is insensitive to the salinity after the seawater is diluted more than seven times; however, the absolute potential increases with dilution. As shown in **Fig. 6(A)**, dilution strongly affects the expansion of the diffuse layer, consequently causing more negative potentials. The proposed crude oil/brine interface at high and low salinities are schematically presented in **Fig. 7** along with the potential distribution, and the surface complexation modelling parameters for crude oil at a low salinity are summarised in **Table 5**. Dilution does not significantly change the concentrations of surface species (-COOH, $-COO^-$, $-COOCa^+$, and $-COOMg^+$), but it causes the potentials to become more negative at each plane due to the decreasing ionic strength. The increases in the potentials and the electrical triple-layer expansion as result of the lowered ionic strength affect the interaction of oil with the rock surface. It was shown that the

potential at the mineral/brine interface is highly negative at a low salinity [25, 27, 44]. This negative electrical potential can create a large repulsive force with crude oil and enhance the oil detachment from the mineral surface, leading to more water-wet conditions. In addition, the ions are more hydrated in the diluted solution than they are in a high-salinity solution, which may also support water-wet conditions [45-46]. Thus, the increase of surface potential at the crude oil/brine interface and the electrical triple-layer expansion are the more pronounced mechanisms for wettability alteration at a low salinity than the dissociation of -COOH and the adsorption of ions on the -COOH surface.

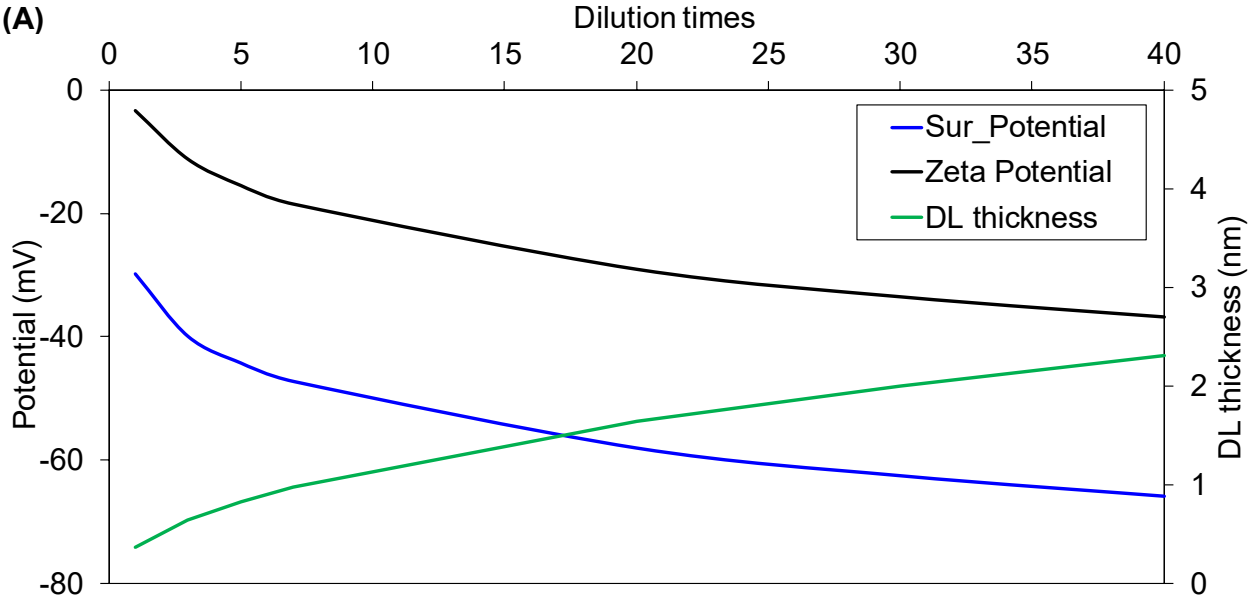

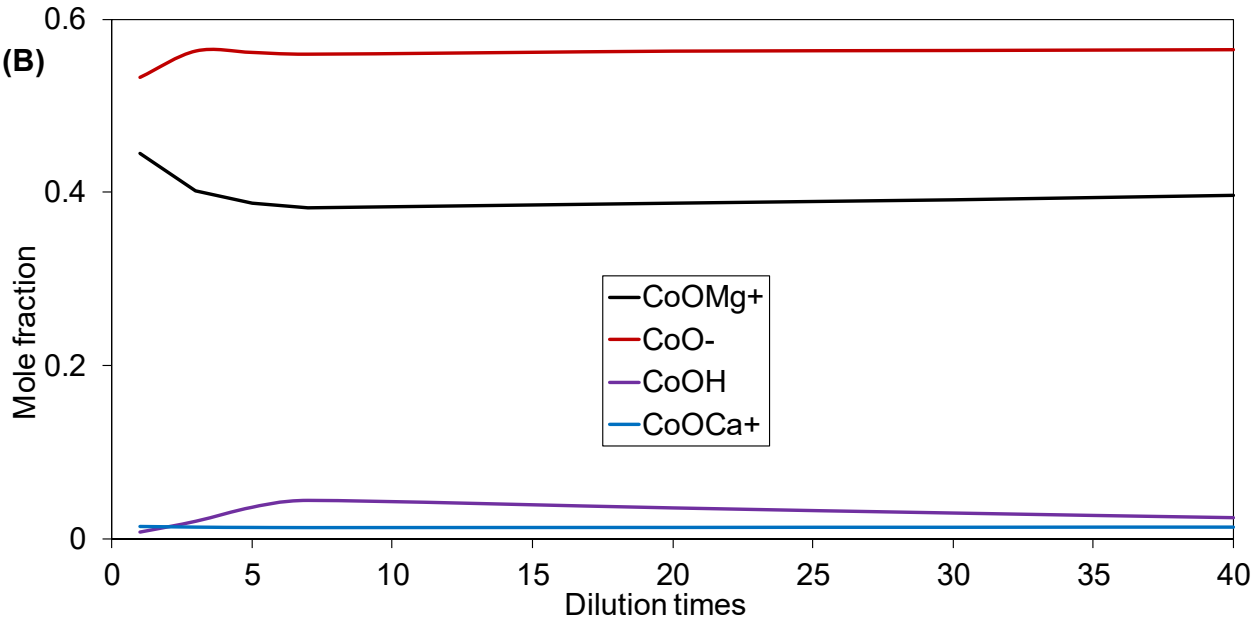

394

395 **Fig. 6.** Simulated (A) surface potential, zeta potential, and diffuse layer thickness; (B) molar fraction

396 of surface species, as a function of dilution times at the crude oil/seawater interface

397

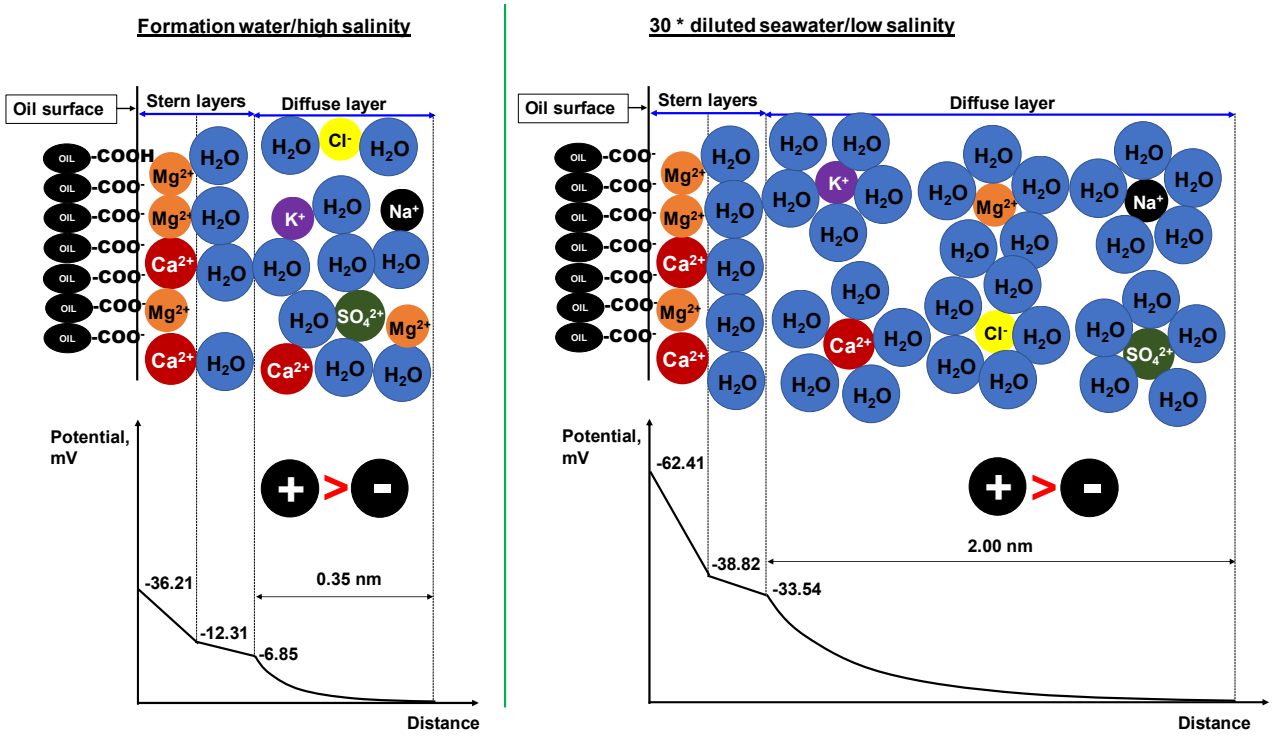

398

399 **Fig. 7.** Illustration of ionic and potential distributions at the crude oil/brine interface

400

401

402

Table 5

Determined surface complexation parameters of crude oil

	Value
-COOH surface site density (sites/nm^2)	0.47
Specific surface area of oil in water (m^2/g of resins)	0.50±0.1
-COOH ↔ -COO$^-$ + H$^+$	*log_k* at 50 ºC = -5.6
-COOH + Ca^{2+} ↔ -COOCa$^+$ + H$^+$	*log_k* at 50 ºC = -4.8±0.1
-COOH + Mg^{2+} ↔ -COOMg$^+$ + H$^+$	*log_k* at 50 ºC = -3.9±0.05
C1	3.10
C2	2.25

4. Conclusions

The crude oil/brine interface was studied using a triple-layer surface complexation model. The model permits the specification of the charge distribution in each plane due to the dissociation of the surface functional groups of crude oil and the adsorption of calcium and magnesium ions onto them. Only the carboxyl group (-COOH) contributes to the charge development of the crude oil emulsion in various solutions. The density of the carboxyl group and the associated equilibrium constants for the dissociation and adsorption of calcium and magnesium were determined by fitting the experimental zeta potential data to those of the simulation. The independence of the zeta potential at a high pH and constant ionic strength due to the complete dissociation of the carboxyl group allowed the determination of its density, while the equilibrium constant for dissociation was calculated from the pH-dependent zeta potential. The estimated values were verified by predicting the zeta potential of the crude oil emulsion at different pH levels in two solutions with different ionic strengths. These values were used to model the interactions of calcium and magnesium with the carboxyl group. Four different cases for the positions of calcium and magnesium near the carboxyl group were considered to estimate the equilibrium constants of adsorption. The determined equilibrium constants were

verified for the emulsion with varying calcium or magnesium concentrations at a constant pH and ionic strength. Separately determined surface complexation modelling parameters were used to predict the zeta potential of crude oil in seawater and formation water as a function of the dilution times. The simulation results agreed well with experimental data, which demonstrates that the model is capable of predicting the interface properties. The proposed model was used to understand the effects of LSWF. A decrease in the salinity causes the surface potential to become more negative and expands the electrical triple-layer, thus resulting in mixed-wet or mixed-wet to water-wet conditions in the reservoir for EOR.

References

[1] Afekare DA, Radonjic M. From Mineral Surfaces and Coreflood Experiments to Reservoir Implementations: Comprehensive Review of Low-Salinity Water Flooding (LSWF). Energy and Fuels 2017;31:13043–62.

[2] Sohal MA, Thyne G, Søgaard EG. Review of Recovery Mechanisms of Ionically Modified Waterflood in Carbonate Reservoirs. Energy and Fuels 2016;30:1904–14.

[3] Sheng JJ. Critical review of low-salinity waterflooding. J Pet Sci Eng 2014;120:216–24.

[4] Al-Shalabi EW, Sepehrnoori K. A comprehensive review of low salinity/engineered water injections and their applications in sandstone and carbonate rocks. J Pet Sci Eng 2016;139:137–61.

[5] Morrow N, Buckley J. Improved Oil Recovery by Low-Salinity Waterflooding. J Pet Technol 2011;63:106–12.

[6] Shariatpanahi SF, Strand S, Austad T. Evaluation of water-based enhanced oil recovery (EOR) by wettability alteration in a low-permeable fractured limestone oil reservoir. Energy and Fuels 2010;24:5997–6008.

[7] Austad T, Shariatpanahi SF, Strand S, Black CJJ, Webb KJ. Conditions for a low-salinity Enhanced Oil Recovery (EOR) effect in carbonate oil reservoirs. Energy and Fuels, vol. 26,

2012, p. 569–75.

[8] Alameri W, Teklu TW, Graves RM, Kazemi H, AlSumaiti AM. Wettability Alteration During Low-Salinity Waterflooding in Carbonate Reservoir Cores. SPE Asia Pacific Oil Gas Conf. Exhib., 2014.

[9] McMillan MD, Rahnema H, Romiluy J, Kitty FJ. Effect of exposure time and crude oil composition on low-salinity water flooding. Fuel 2016;185:263–72.

[10] Yousef AA, Al-Saleh SH, Al-Kaabi A, Al-Jawfi MS. Laboratory Investigation of the Impact of Injection-Water Salinity and Ionic Content on Oil Recovery From Carbonate Reservoirs. SPE Reserv Eval Eng 2011;14:578–93.

[11] Suijkerbuijk B, Hofman J, Ligthelm DJ, Romanuka J, Brussee N, van der Linde H, et al. Fundamental Investigations into Wettability and Low Salinity Flooding by Parameter Isolation. SPE Improv Oil Recover Symp 2013:1–23.

[12] Qiao C, Johns R, Li L. Modeling Low-Salinity Waterflooding in Chalk and Limestone Reservoirs. Energy and Fuels 2016;30:884–95.

[13] Aladasani A, Bai B, Wu Y, Salehi S. Studying low-salinity waterflooding recovery effects in sandstone reservoirs. Journal of Petroleum Science and Engineering 2014; 120:39-51.

[14] Hua Z, Li M, Ni X, Wang H, Yang Z, Lin M. Effect of injection brine composition on wettability and oil recovery in sandstone reservoirs. Fuel 2016;182:687–95.

[15] Mahzari P and Sohrabi M. Crude oil/brine interactions and spontaneous formation of micro-dispersions in low salinity water injection. Paper SPE-169081 presented at the SPE Improved Oil Recovery Symposium held in Tulsa, Oklahoma, USA, 12–16 April 2014.

[16] Sohrabi M, Mahzari P, Farzaneh S. A, Mills J. R, Tsolis P, and Ireland S, Novel insights into mechanisms of oil recovery by use of low-salinity-water injection, SPE Journal, April 2017, 407-416.

[17] Alvarado V, et.al. Impact of polar components on crude oil-water interfacial film formation: A mechanisms for low-salinity waterflooding, Paper SPE-170807 presentation at the SPE Annual

473 Technical Conference and Exhibition held in Amsterdam, The Netherlands, 27–29 October
474 2014.
475 [18] Jackson MD, Vinogradov J, Hamon G, Chamerois M. Evidence, mechanisms and improved
476 understanding of controlled salinity waterflooding part 1: Sandstones. Fuel 2016;185:772–93.
477 [19] Mahani H, Keya AL, Berg S, Bartels WB, Nasralla R, Rossen WR. Insights into the mechanism
478 of wettability alteration by low-salinity flooding (LSF) in carbonates. Energy and Fuels
479 2015;29:1352–67.
480 [20] Austad T, RezaeiDoust A and Puntervold T. Chemical Mechanism of Low Salinity Water
481 Flooding in Sandstone Reservoirs. paper SPE 37236 presented at the 2010 SPE Improved Oil
482 Recovery Symposium held in Tulsa, Oklahoma, USA, 24–28 April 2010.
483 [21] Tian H, Wang M. Electrokinetic mechanism of wettability alternation at oil-water-rock
484 interface. Surf Sci Rep 2018;72:369–91.
485 [22] Chow RS, Takamura K. Electrophoretic mobilities of bitumen and conventional crude-in-water
486 emulsions using the laser Doppler apparatus in the presence of multivalent cations. J Colloid
487 Interface Sci 1988;125:212–25.
488 [23] Buckley JS, Takamura K. Influence of Electrical Surface Charges on the Wetting Properties of
489 Crude Oils. Soc Pet Eng 1987:332–40.
490 [24] Myint PC, Firoozabadi A. Thin liquid films in improved oil recovery from low-salinity brine.
491 Curr Opin Colloid Interface Sci 2015;20:105–14.
492 [25] Nasralla RA, Nasr-El-Din HA. Impact of cation type and concentration in injected brine on oil
493 recovery in sandstone reservoirs. J Pet Sci Eng 2014;122:384–95.
494 [26] Matthew D. Jackson, Dawoud Al-Mahrouqu & Jan Vinogradov. Zetapotential in oil-water-
495 carbonate systems and its impact on oil recovery during controlled salinity water-flooding.
496 Scientific Reports 2016.1-13.
497 [27] Xie Q, Liu Y, Wu J, Liu Q. Ions tuning water flooding experiments and interpretation by
498 thermodynamics of wettability. J Pet Sci Eng 2014;124:350–8.

499 [28] Xie Q, Saeedi A, Pooryousefy E, Liu Y. Extended DLVO-based estimates of surface force in
500 low salinity water flooding. J Mol Liq 2016;221:658–65.
501 [29] Hirasaki GJ. Wettability: Fundamentals and Surface Forces. SPE Form Eval 1991;6:217–26.
502 [30] Brady P V., Krumhansl JL. A surface complexation model of oil-brine-sandstone interfaces at
503 100 ºC: Low salinity waterflooding. J Pet Sci Eng 2012;81:171–6.
504 [31] Brady P V., Morrow NR, Fogden A, Deniz V, Loahardjo N, Winoto A. Electrostatics and the
505 low salinity effect in sandstone reservoirs. Energy and Fuels 2015;29:666–77.
506 [32] Eftekhari AA, Thoms27-28en K, Stenby EH, Nick HM. Thermodynamic Analysis of Chalk-
507 Brine-Oil Interactions. Energy and Fuels 2017;31:11773–82.
508 [33] Xie Q, Brady P V., Pooryousefy E, Zhou D, Liu Y, Saeedi A. The low salinity effect at high
509 temperatures. Fuel 2017;200:419–26.
510 [34] Chen Y, Xie Q, Sari A, Brady P V., Saeedi A. Oil/water/rock wettability: Influencing factors
511 and implications for low salinity water flooding in carbonate reservoirs. Fuel 2018;215:171–7.
512 [35] Qiao C, Li L, Johns RT, Xu J. A Mechanistic Model for Wettability Alteration by Chemically
513 Tuned Waterflooding in Carbonate Reservoirs. SPE J 2015:17.
514 [36] Mahzari P, Sohrabi M, Cooke A. J, Carnegie A, Direct pore-scale visualization of interactions
515 between different crude oils and low salinity brine, J Pet Sci Eng 2018;166:73–84.
516 [37] Hiemstra T, Wolthers M. A Surface StructuralAapproach to Ion Adsorption: The Charge
517 Distribution (CD) Model. J Colloid Interface Sci 1996;179:488–508.
518 [38] Rahnemaie R, Hiemstra T, Riemsdijk, W. H, A new surface structural approach to ion
519 adsorption: Tracing the location of electrolytes, J Colloid Interface Sci 2006;293:312-321.
520 [39] Parkhurst BDL, Appelo C a J. User's Guide To PHREEQC (version 2) — a Computer Program
521 for Speciation, and Inverse Geochemical Calculations. Exch Organ Behav Teach J 1999;D:326.
522 [40] Kunieda, M et.al. Self-accumulation of aromatics at the oil-water interface through weak
523 hydrogen bonding, J. AM. CHEM. SOC. 2010, 132, 18281–18286.
524 [41] Andrews A. B, et.al. Molecular orientation of asphaltenes and PAH model compounds in

525 Langmuir-Blodgett films using sum frequency generation spectroscopy, Langmuir, 2011, 27,
526 6049-6058.
527 [42] Ruiz-Morales, Y and Mullins, O. C. Coarse-grained molecular simulations to investigate
528 asphaltenes at the oil-water interface, energy & fuel, 2015, 29, 1597-1609.
529 [43] Shehata, A. M.; Nasr El-Din, H. A. Spontaneous Imbibition Study: Effect of Connate Water
530 Composition on Low-Salinity Waterflooding in Sandstone Reservoirs. Society of Petroleum
531 Engineers: Houston, TX, 2015.
532 [44] Takahashi S, Kovscek AR. Wettability estimation of low-permeability, siliceous shale using
533 surface forces. J Pet Sci Eng 2010;75:33–43.
534 [45] Nicolini JV, Ferraz HC, Borges CP. Effect of seawater ionic composition modified by
535 nanofiltration on enhanced oil recovery in Berea sandstone. Fuel 2017;203:222–32.
536 [46] Yang G, Chen T, Zhao J, Yu D, Liu F, Wang D, et al. Desorption Mechanism of Asphaltenes
537 in the Presence of Electrolyte and the Extended Derjaguin-Landau-Verwey-Overbeek Theory.
538 Energy and Fuels 2015;29:4272–80.